Energy Reports 9 (2023) 163–177

Contents lists available at ScienceDirect

Energy Reports

journal homepage: www.elsevier.com/locate/egyr

Research paper

Analysis of control strategies for smoothing of solar PV fluctuations with storage devices☆

G.V. Brahmendra Kumar [a,*,1], Palanisamy K. [a,1], Sanjeevikumar P. [b,1], S.M. Muyeen [c,*,1]

[a] School of Electrical Engineering, Vellore Institute of Technology, Vellore, 632014, India
[b] Department of Electrical Engineering, University of South-Eastern Norway, Norway
[c] Department of Electrical Engineering, Qatar University, Doha 2713, Qatar

ARTICLE INFO

Article history:
Received 14 July 2022
Received in revised form 13 November 2022
Accepted 26 November 2022
Available online xxxx

Keywords:
DC microgrid
Fluctuations
Renewable energy sources
Storage devices
Smoothing controls
Battery
Supercapacitor

ABSTRACT

The irradiation variations caused by cloud changes can cause rapid power fluctuations in large photovoltaic (PV) plants. The increased PV power share of the grid adversely affects the quality of power and the reliability of the power supply. Energy storage systems (ESSs)are often used to mitigate power fluctuations in the grid through various control algorithms. These algorithms create an ESS power reference that opposes the variations of the PV and reduces them to an acceptable value. Despite their everyday use, there have been few performance comparisons among the various methods, especially battery status, and the battery can operate in several systems with various smoothing methods. The paper aims to analyze the ramp-rate and step-rate control methods for smoothing solar PV fluctuations based on the irradiation profiles in a DC microgrid (MG) environment. The battery in the system operates as a continuous energy application, and a supercapacitor (SC) is used to remove transients in the battery system. The combined battery-SC coordinated system improves the performance of the DC microgrid system. The battery cycle analysis and depth are conducted using the well-established Coulomb counting technique. MATLAB/Simulink validates the simulation results, and the OP-5700 HIL test bench conducts real-time results.

1. Introduction

In remote locations, solar and wind energy sources are regarded as economically viable renewable energy sources (RESs) (Brahmendra Kumar and Palanisamy, 2019). The load demand is deficient in remote areas (RAs). Therefore, supplying power from the grid is unnecessary because of transmission and daily maintenance costs. As a result, the standalone power system (SPS) acts as the most appropriate power source in the RAs and provides benefits such as lower operating and maintenance costs. RESs alone cannot meet the load demand in RAs because of the varying nature of RESs and load demand. SPSs rely heavily on ESSs to provide a constant power supply to loads powered by intermittent sources such as wind and solar (Kumar and Palanisamy, 2021; Tahir et al., 2022; Kumar and Palanisamy, 2020).

The ESS installation significantly impacts a PV system's energy and economic balance and is critical for future viability due to its inflated cost and lower shelf-life of PV systems. This emphasizes the importance of ESS parameters such as energy efficiency, losses, and cycling decay. Any decrease in ESS capacity and charge/discharge cycles reduces the investment required to install and maintain the ESS (Brahmendra Kumar and Palanisamy, 2021). Therefore, the control strategy chosen to smooth out fluctuations becomes a key decision. However, various control strategies are available depending on the maximum fluctuation limit to keep the fluctuations below that limit.

The literature (Prabha et al., 2019) contains three commonly used control strategies: ramp-rate (RR), step-rate (SR), and moving-average (MA) controls. The main asset of MA is that when the system has an ideal converter and a battery, the mean value of energy in the ESS should be the same at the beginning and end of each day. The ESS is discharged with a value equal to the energy lost in the processes of charge/discharge. However, the effectiveness of system storage is poor, and storage system losses are high. Several control strategies are available in Patel et al. (2020) and Zhang et al. (2021), but these do not smooth the fluctuations in the PV system and cause very large ESS in short periods. The mitigation of fluctuations using the MA control and a first-order low-pass filter is also discussed. The ESS SoC can be

☆ Funding: No source of funding for this research activity.
* Corresponding authors.
E-mail addresses: brahmendrakumar.g@gmail.com (G.V.B. Kumar), kpalanisamy@vit.ac.in (Palanisamy K.), sanjeevi_12@yahoo.co.in (Sanjeevikumar P.), sm.muyeen@qu.edu.qa (S.M. Muyeen).
[1] All authors were involved equally in making the research article in its current form.

https://doi.org/10.1016/j.egyr.2022.11.176

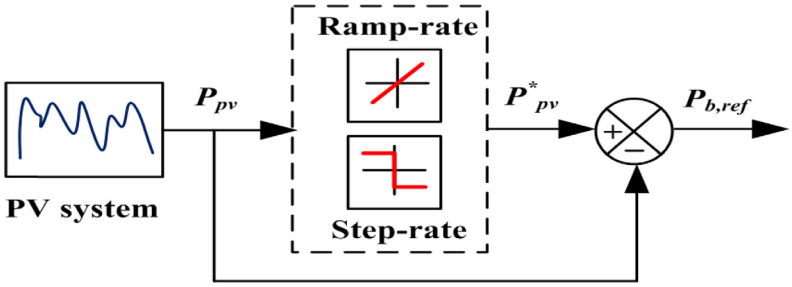

Fig. 1. Smoothing control block diagram.

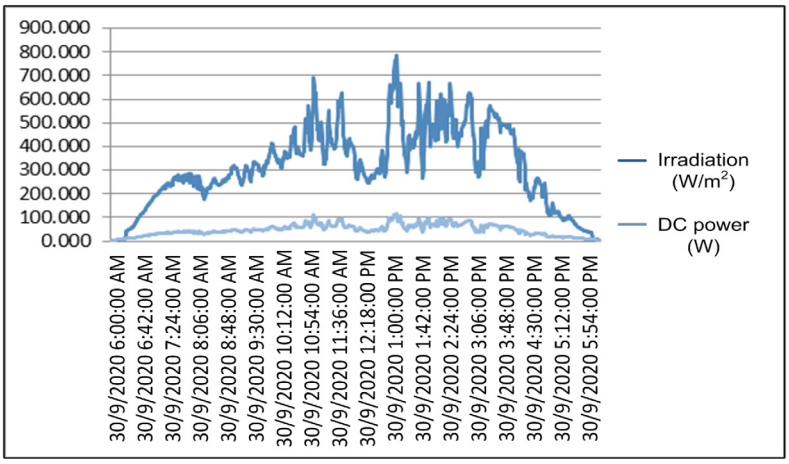

Fig. 2. Severe PV variations on a day.

maintained over the range by modifying the ESS power output. There is no significant analysis of the impact of these strategies on ESS charge/discharge cycles, cycling degradation, SoC levels, and voltage regulation.

The dynamic state analysis of voltage control was performed in Mahmud et al. (2017), but no limiting factor was measured in the BESS's State of Charge (SoC). A voltage-based storage control for distributed solar PV generation with battery systems is discussed (Zeraati et al., 2018). The article (Zeraati et al., 2018) proposes voltage regulation to reduce the slow fluctuation in PV production. However, practical problems like limited BESS capacity, sudden fluctuations in PV generation, etc., were not considered. In Chen et al. (2019), the ESS only handles power ramp-down. In this strategy, the battery discharges during the day and charges slowly at night. Initial SoC can be set high to reduce capacity and charge cycles. Batteries degrade from frequent discharge/charge cycles. Uncertain charge/discharge during control makes estimating battery capacity challenging, leading to redundant assessment (Beltran et al., 2019). In Pranith et al. (2022), an adaptive control algorithm with the MAC method reduces the distribution system intermittency. The ESS SoC can be maintained over the range by modifying the ESS power output. There is no unique PV smoothing strategy because it is determined by many factors, including the cost, the response time of the resource compensation, and the system operating policy. The time to transfer data can also make the output less smooth or cause more fluctuations (Pranith et al., 2022).

Using ESS for smoothing control has been the subject of many studies in the existing literature (Sukumar et al., 2018). This method improves power generation efficiency, as no energy is lost in the conversion process. However, using ESS requires advanced communication systems, reducing battery life and significantly increasing PV system costs. Alternative methods for monitoring passing clouds include ground sensors or sky-camera systems. These methods cannot achieve such a high average accuracy because the shadow map obstructs it at ground level. However, both methods require additional hardware and communication systems, which increases the system's capital cost (Saleh et al., 2018). Recently, power curtailment (PC) techniques have been studied (Solomon et al., 2019). Depending on the specifics of each installation, a PC is a viable option despite the waste of energy because it requires a low initial investment. It is important to note that PC and storage do not always substitute for each other; Sometimes, a hybrid approach is the most cost-effective solution (Li et al., 2020). Because of the high cost and short life of batteries, active PC has been discussed in Lin et al. (2020). This simple, low-cost technique achieves RRC without ESSs. A PV system operates at a sub-optimal power level instead of at its peak power. Part of the PV electricity can be saved for smooth output power. However, the APC mechanism controls only RR up, not RR down.

According to the literature above, achieving optimal and accurate smoothing is the most important factor in managing PV power fluctuations. The algorithms for controlling PV and ESS and coordinating their use are also crucial. In Neto et al. (2020), a system for power management in the DC MG with virtual inertia and a mode of operation based on the voltage distribution is proposed. However, during transient conditions, the strategy failed to maintain a DC link voltage at the required voltage level. A new control strategy for the hybrid DC grid is proposed in Mardani et al. (2019). This technique can eliminate the high current and power pulsations but suffer from more voltage deviations. In Xu et al. (2017) and Kollimalla et al. (2017), a power coordination

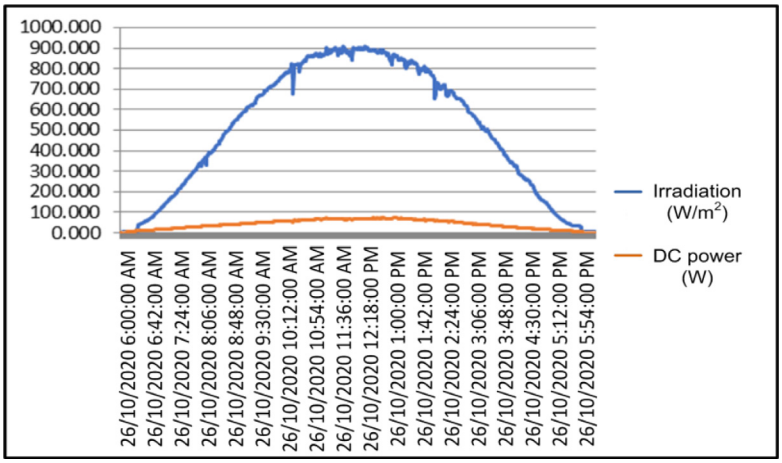

Fig. 3. Normal PV variations on a day.

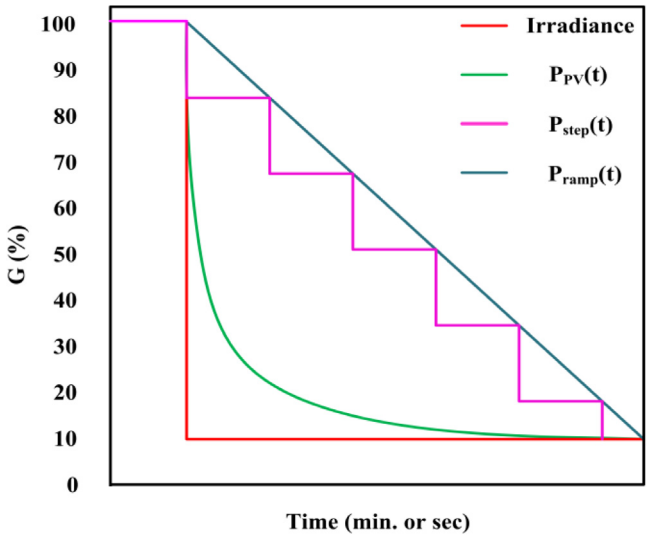

Fig. 4. PV power fluctuation model with RR and SR controls.

algorithm between the RES and the Hybrid Energy Storage System (HESS). This algorithm shows that the SC is of greater importance than the BESS but does not discuss battery and SC coordination for concurrent operations. The RR-based control method (Kumar et al., 2020) was proposed to reduce PV power fluctuations. However, there is no analysis to choose a better smoothing method for improving efficiency in the integrated renewable grid system. The authors proposed a control approach based on a power filter for wind power applications in Lamsal et al. (2019), in which low-frequency components are moved to the BESS and the other power components to the SC. However, there are no apparent reasons for the power filter design to deal with rapid power variations. A PV system with HESS for DC MG is proposed in Kotra and Mishra (2019) and Sathishkumar et al. (2012). It generates power based on the maximum power obtained from the PV system, thereby increasing the capacity and size of the ESS. Also, it requires more setting time to restore a stable DC link voltage. The approach based on lower and higher-frequency power components is used in Cao et al. (2018), where the BESS provides the average demand, and the SC provides the transient power fluctuations. However, the slow dynamics of the BESS do not improve the HESS dynamic performance.

Table 1
Comparison of smoothing control methods.

Control method	Storage time effectiveness	Losses in SS	Degradation of the cycle
SRC (Prabha et al., 2019)	Average	Average	≤2%
RRC (Prabha et al., 2019)	High	Low	<2%
MA (Pranith et al., 2022)	Low	High	∼10%
DMA (Pranith et al., 2022)	Low	High	∼10%
LPF (Kotra and Mishra, 2019)	Low	Average	∼1%

The above articles discussed various techniques for controlling solar PV power output changes based on the solar PV generator input or sequential inputs. Several variables are required to prevent the PV energy loss caused by the output of the BESS, which always depends on the previous output of the BESS. The MA method and its adjustments have been discussed in Prabha et al. (2019), and results depend on time window selection. These results are less desirable due to their higher dependence on data from the previous generation. In Chen et al. (2019), the RRC was based on the percentage change in the ramp-rate relative to PV generation. In Schnabel and Valkealahti (2016), the low-pass filter (LPF) method has been examined. If the limit of the smoothing control is less than 5%/min, the demand for storage system capacity increases significantly. Different results are achieved by the lagging and double-MA (DMA) methods based on window size and solar PV data. The DMA method results in a smoother output than other moving average techniques. The SR control is significant if the RS strictly allows maximum value within the time window. The SR control is used to reduce the size of the ESS and lower ESS degradation compared to the MA method. The critical advantage of RRC is that it only operates when the fluctuation is higher than the maximum permissible RR value. The smoothing control comparison is listed in Table 1.

The paper aims to analyze RR and SR controls for irregular solar PV fluctuations to choose the best smoothing method.

- This paper also discusses the drawbacks of literacy articles for limiting fluctuations in PV power, practical usage of HESS, removing stress on the ESS, and increasing system lifetime.
- These variations can be limited through RR/SR controls and achieve fast DC-link voltage regulation.
- A new control mechanism is proposed for coordination between BESS and SC.
- The proposed strategy's main advantage is overcoming the slow response of battery storage by diverting power surges to the system SC.

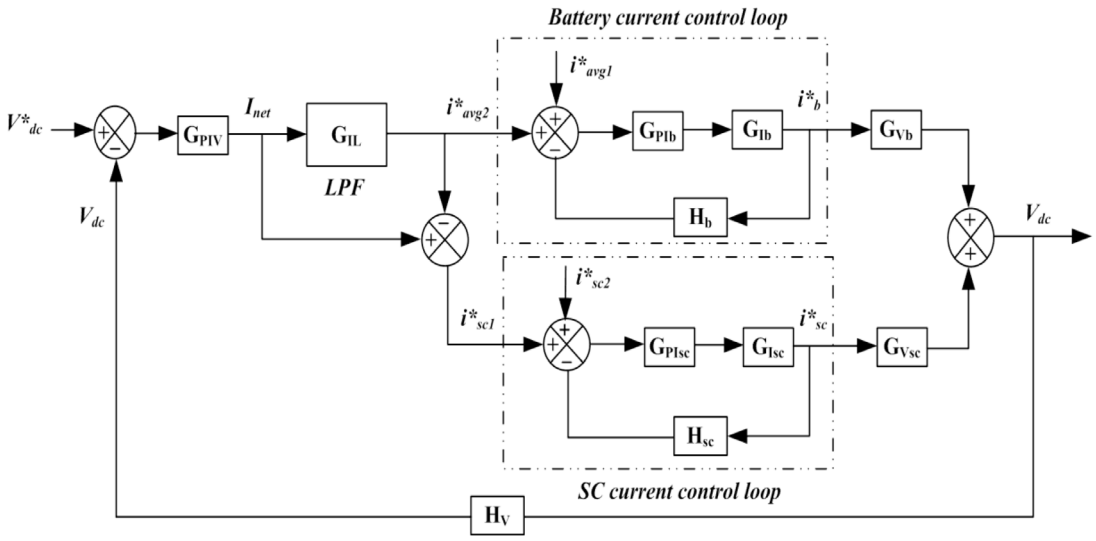

Fig. 5. Small-signal modeling of proposed HESS.

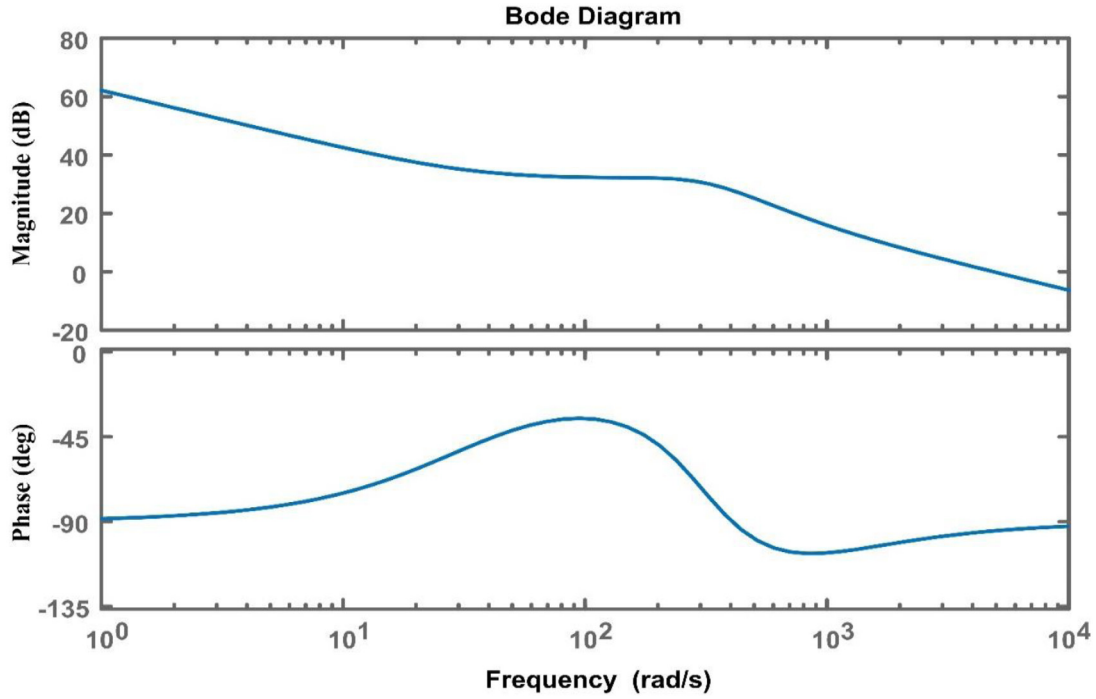

Fig. 6. Bode diagram of the current control loop for the battery.

- The SC provides the battery error component current in the proposed control strategy.
- This feature makes it easier to control the DC grid voltage and reduces the stress on the battery, which makes the battery last longer.
- RR control is the best smoothing method regardless of setting time (T_s), peak overshoot (M_p), or change in DC voltage (ΔV_{dc}). It regulates DC link voltage in 199 ms for load changes.

The following sections are Section 2 represents the integration of PV power with smoothing control. Section 3 deals with the small-signal modeling of the proposed HESS. The configuration and control of the proposed system are discussed in Section 4. Section 5 deals with the HIL results, followed by the conclusions presented in Section 6.

2. Integration of PV power smoothing control

PV power fluctuates significantly because of its irregularity, uncontrollability, and climate variation. The injection of PV power causes power quality issues such as voltage fluctuations and instability in the distribution system. These issues can be mitigated using efficient ESS, and smoothing control can smooth the solar system's PV energy. Smoothing control keeps variations in PV power within specified limits and ensures the network's stability (Brahmendra Kumar et al., 2018).

Fig. 1 shows the smoothing control block diagram applied to extreme solar PV variations on the day given in Fig. 2.

The control algorithm reduces the $P_{PV}(t)$ fluctuations to the maximum allowed level (r_{max}) for each sampling period, and the resulting smoothing power (P^*_{PV}) is injected into the grid. The difference between $P_{PV}(t)$ and $P^*_{PV}(t)$ represents the power

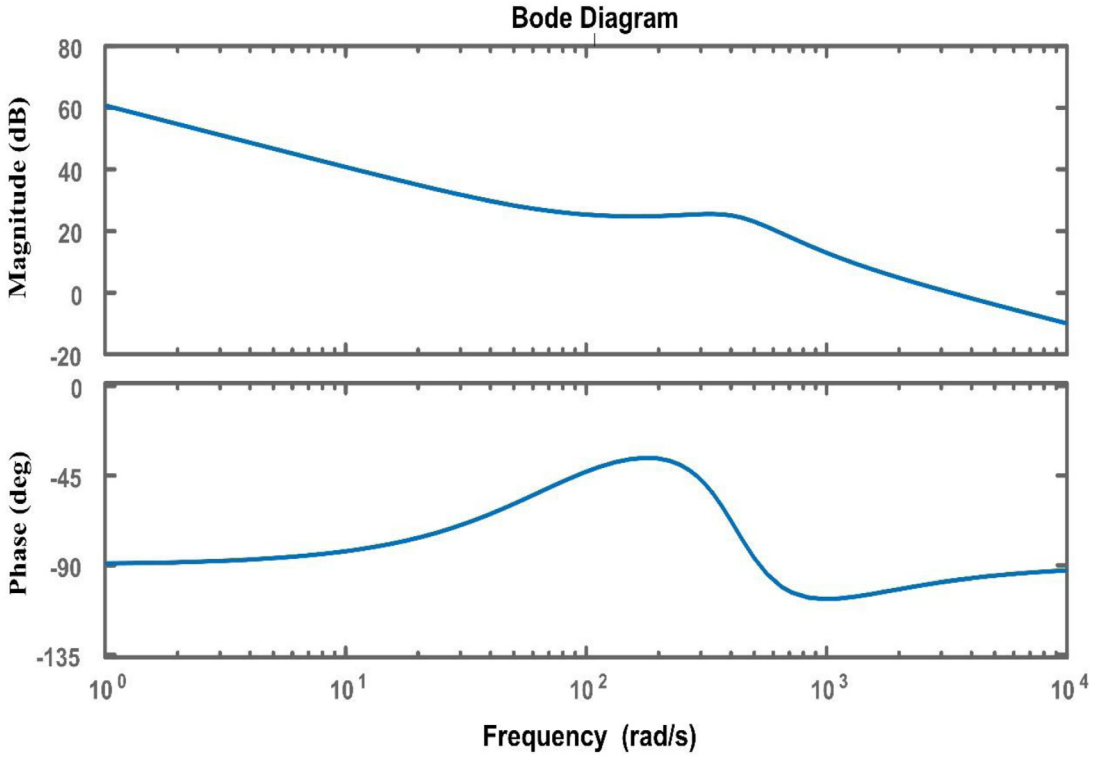

Fig. 7. Bode diagram of the current control loop for SC.

setpoint of the ESS that can be delivered ($P_{ESS} > 0$) or absorbed by the ESS ($P_{ESS} < 0$). During normal solar variability, the variation is not severe. In the worst-case scenario, the fluctuation of the passing cloud can be severe. Based on Fig. 2, 70 to 90 percent power changes were observed in severe fluctuations. Periodic 1-minute data from 6 a.m. to 6 p.m. during the day are presented in Figs. 2 and 3 to observe the changes in the PV output power. The fluctuation model of PV output power with RR and SR controls is presented in Fig. 4.

Where G is the % change in irradiance levels, $P_{ramp}(t)$ and $P_{step}(t)$ are the power delivered to the grid with RR and SR controls. The battery power (P_b) difference between PV output power and the power delivered to the grid with smoothing control.

3. Small-signal modeling of proposed HESS

The small-signal modeling of the proposed HESS is presented in Fig. 5. A Low Pass Filter (LPF) ensures that power is shared between the battery and the SC (Gundumalla and Eswararao, 2018). G_{Ib} and G_{Isc} are the parameters of the battery and SC control transfer function that control the current through inductors. Based on the SC power phase, the controller of PI is tuned because the SC has higher charge/discharge rates than the battery. To avoid oscillations, the SC's internal loop bandwidth (BW) is restricted to $f_{sw}/6$ (Kollimalla et al., 2017). The BW of the battery current loop is kept below the SC current loop BW, i.e., at $f_{sw}/10$, to divert the fast-changing transients to the SC.

The feedback system is tuned with two PI controls. The typical representation of PI is as follows:

$$PI_a = KP_a + \frac{KI_a}{s} \tag{1}$$

where a represents the PI gains of the battery (b) and a supercapacitor (sc) for the inner control loop. Here, H_B and H_{sc} are the transfer function's feedback parameters to be unity. Because they are complementary to both converters, these processes lead to errors. The control transfer function of the battery inductor current is specified by (Kollimalla et al., 2017),

$$G_{ib} = \frac{V_0 C_b s + 2\frac{V_0}{R_L}}{L_b C_b s^2 + \frac{L_b}{R_L} s + (1 - D_b)^2} \tag{2}$$

In the battery converter, the following equation takes the current control loop:

$$G_{PIb} = K_{Pb} + \frac{K_{Ib}}{s} \tag{3}$$

The current controller open-loop TF of the battery is taken by,

$$G_{olb} = G_{PIb} G_{Ib} H_b \tag{4}$$

where K_{pb} and K_{Ib} are the compensator PI gains, H_b is the current sensor gain of the battery. The control transfer function of the SC inductor current is given as follows (Kollimalla et al., 2017),

$$G_{sc} = \frac{V_0 C_{sc} s + 2\frac{V_0}{R_L}}{L_{sc} C_{sc} s^2 + \frac{L_{sc}}{R} s + (1 - D_{sc})^2} \tag{5}$$

The following equation takes the SC converter current control loop,

$$G_{PIsc} = K_{Psc} + \frac{K_{Isc}}{s} \tag{6}$$

The current controller open-loop TF of SC is given as,

$$G_{olsc} = G_{PIsc} G_{Isc} H_{sc} \tag{7}$$

where K_{psc} and K_{Isc} are the compensator PI gains, H_{sc} is the current sensor gain of the SC. The total load voltage can be taken as,

$$v_0(s) = (i_b(s) + i_{sc}(s)) R_L \tag{8}$$

V_o, L_b, and L_{sc}, C_b and C_{sc}, D, R_L are the output voltage, battery and SC inductances, battery and SC capacitances, duty ratio, and load resistance. The bode diagram of the battery and SC current control loops are illustrated in Figs. 6 and 7.

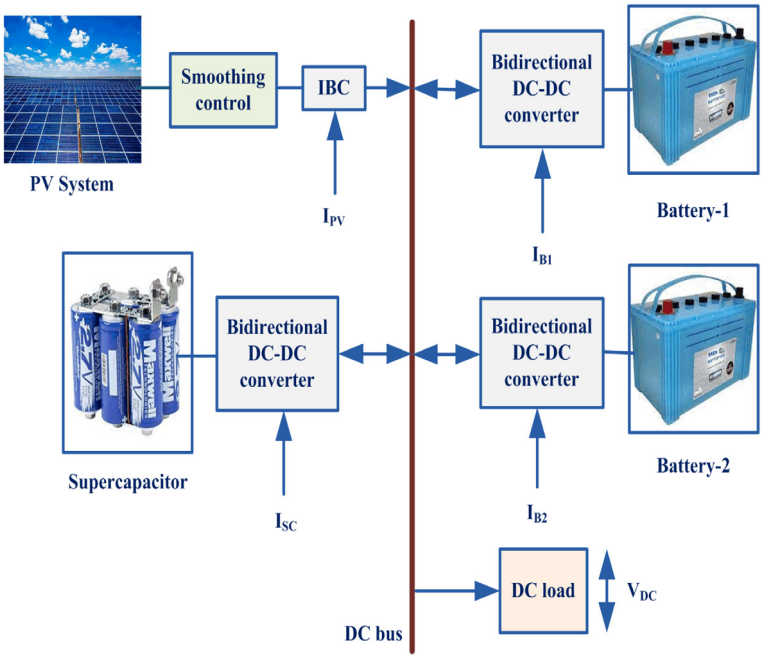

Fig. 8. Block diagram of DC MG system.

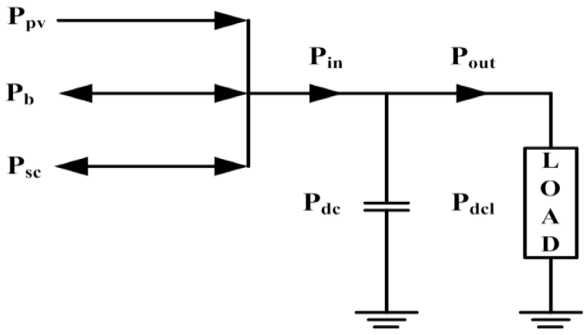

Fig. 9. Power flows in the DC MG system.

4. Configuration and control of the proposed DC MG system

The block diagram of the DC MG comprising PV and HESS is presented in Fig. 8. The PV system and HESS are associated with an interleaved boost converter (IBC) and bi-directional converters. The IBC is used to reduce conduction losses and improve the transformation ratio. Hence, energy savings can improve the system's effectiveness (Kumar and Palanisamy, 2019). PV and HESS converters work in parallel and are required to maintain a constant power balance in the DC grid. The smoothing and DC-link controls generate the reference signals for batteries. The system cannot maintain a constant voltage in a network because it is connected to the grid by current-controlled converters. Therefore, we must use a controller to maintain a constant voltage on the grid. In Gundumalla and Eswararao (2018), the authors proposed a DC link controller and a storage system that quickly adjusts the DC link voltage when a PV or load power change occurs.

Fig. 9 depicts the different power flows of the DC MG system. The power balance equation of the DC MG is as follows (Kollimalla et al., 2017),

$$P_{in}(t) = P_{dc}(t) + P_{out}(t) \tag{9}$$

$$P_{in}(t) = P_{pv}(t) \pm P_b(t) \pm P_{sc}(t) \tag{10}$$

where P_{pv}(t), P_b(t), P_{sc}(t), P_{dc}(t), and P_{dcl}(t) are the power contributed by the PV system, batteries, SC, DC link capacitor, and DC load, respectively. Where, as long as P_{in}(t) is equal to P_{out}(t), P_{dc}(t) will be zero, such that a constant voltage is maintained whenever there is an imbalance between input and output. The DC-link capacitor charges or discharges, increasing or decreasing the DC link voltage.

Hence, the i^*_{avg} is generated by using the DC-link regulator illustrated in Fig. 10(b), and it is drawn from the following equation (Gundumalla and Eswararao, 2018),

$$i^*_{avg}(t) = \left(\frac{1}{1+s\tau_c}\right) i_{net}(t) \tag{11}$$

where τ_c is the time constant of the filter. The SC transient current (its) is generated by the equation as follows (Cao et al., 2018),

$$i_{trs}(t) = \left(1 - \frac{1}{1+s\tau_c}\right) i_{net}(t) \tag{12}$$

A low-pass filter (LPF) passes the *B1* net current to achieve an average value of the net current required by the *B1* controller. The i^*_{SC1} is generated based on the difference between i^*_{avg} and i_{net} of *B1*. The SoC of the system is measured using the count-Coulomb method in Fig. 10(a). The SoC of the battery system performs significantly and enhances the battery device's efficiency. The initial SoC is considered as 80%. The calculation part of the SoC is given as (Tummuru et al., 2015),

$$SoC_b = SoC_{in} - \frac{1}{3600C_N}\int i_b dt \tag{13}$$

SoC_{in} and C_N are the battery's initial SoC and nominal capacitance, respectively.

5. HIL experimental setup results and discussion

OP5700 HIL was used in Fig. 11 for testing results by RT-LAB, MSOX3014T, PCB-E06-0560, connection devices, and probes. The PCB interfaces the simulation with the real-time controller for data exchange using analogue O/Ps and digital I/Ps. In Fig. 11, the setup of real-time results is presented.

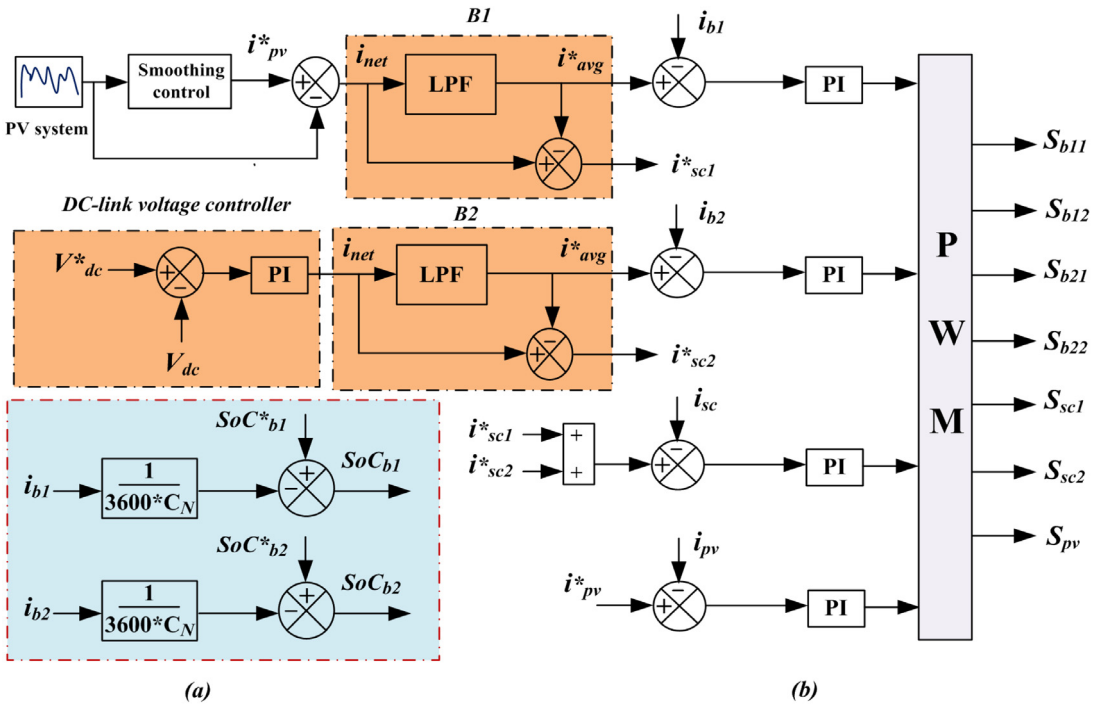

Fig. 10. (a) SoC Coulomb counting control, (b) proposed system control configuration.

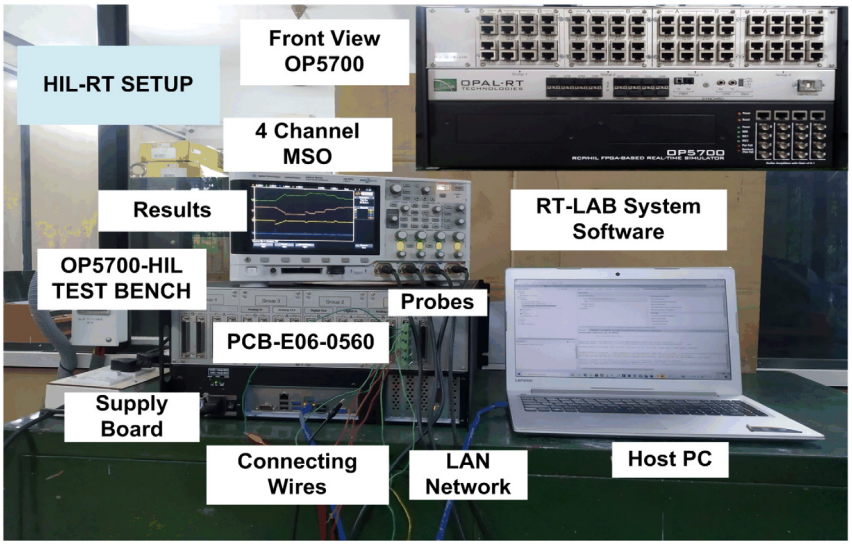

Fig. 11. OP5700-HIL-RT setup.

The system HIL parameters are given in Table 2. Figs. 12, 14, 16, and 18 show the ramp-rate control-based DC MG system results, and Figs. 13, 15, 17, and 19 show the step-rate control-based DC MG system. Figs. 12(a) and 13(a) show the variable PV current. The battery B1 and B2 currents are presented in Figs. 12(b) and (c), 13(b) and (c). The response of SC is shown in Figs. 12(d) and 13(d). The SC helps in reducing rapid changes in B1 and B2 currents. As a result, the stress level in the battery system is reduced. The lifetime of the battery system is increased. The variable DC load is illustrated in Figs. 14(b) and 15(b), and the DC grid voltage response is presented in Figs. 14(a) and 15(a). Table 4 compares the performance of DC link voltage in the RR and SR control methods.

The regulation of DC bus voltage in RR control is as follows compared with the SR control in Figs. 16 and 17,

Case i: There is no variation in PV and load currents from t_0 to t_2; the DC link voltage is maintained constant.

Case ii: During period t_2, PV varies while load current remains constant. The voltage of the DC link is increased to +2 V/div.

Case iii: During the time interval t_3, the load varies while the PV current remains constant. The voltage of the DC link is increased to +1 V/div.

Case iv: PV and load currents vary between t_5. The voltage across the DC link is reduced to −2 V/div.

As a result, it is clear from cases i–iv in Fig. 16(a) for RR control that when there is a sudden change in PV or load, there

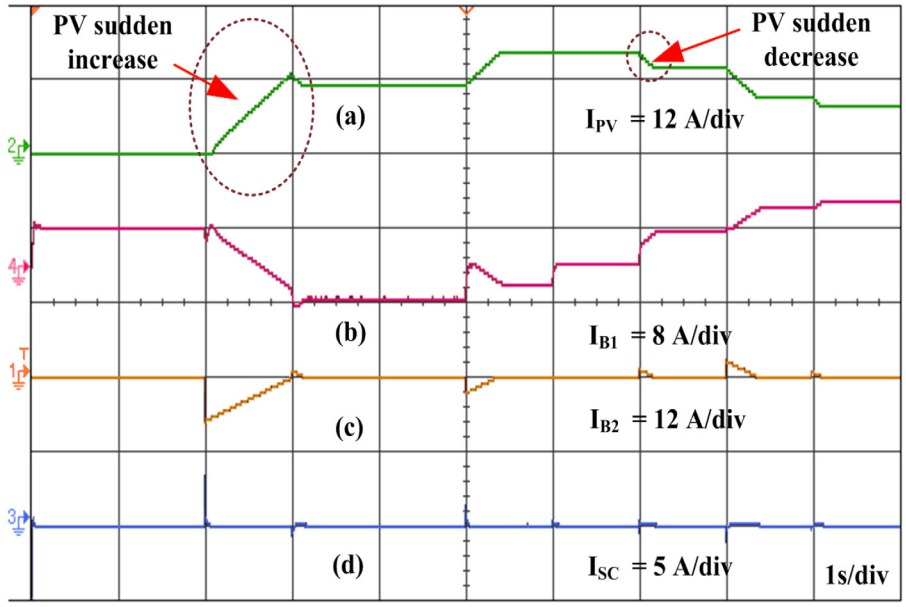

Fig. 12. HIL test-bench results — Ramp-rate control: (a) PV current (V_{DC}), (b) battery-1 current, (c) battery-2 current, (d) SC current.

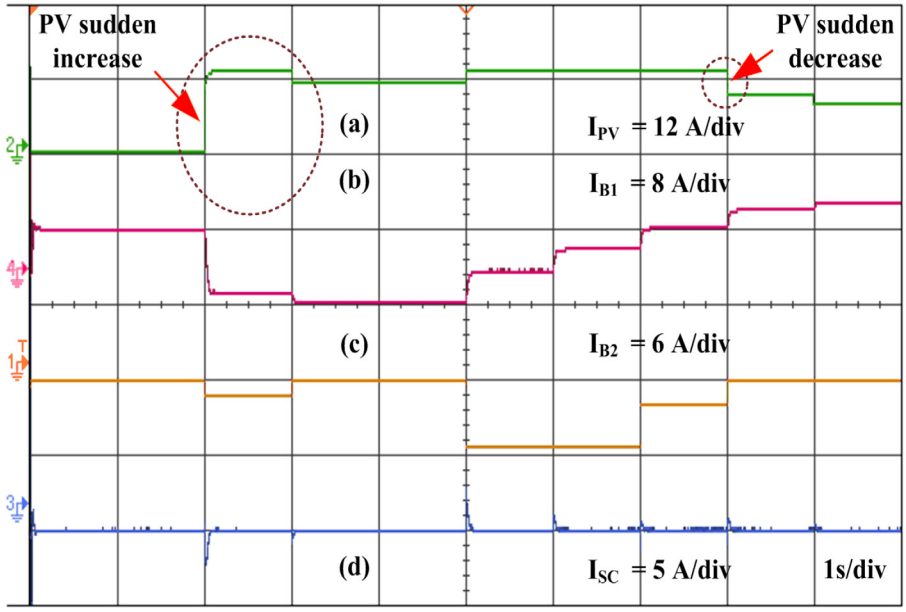

Fig. 13. HIL test-bench results — Step-rate control: (a) PV current (V_{DC}), (b) battery-1 current, (c) battery-2 current, (d) SC current.

Table 2
DC grid HIL parameters.

PV system: Input voltage, solar irradiance; converter parameters	V_{in}, 40 V; I, 1000 W/m^2; L_{pv}, 5 mH; C_{pv}, 500 μF
Battery: Capacity; terminal voltage; no. of batteries in series; Converter parameters	C_b, 12 Ah; V_b, 48 V; 4; L_b, 5 mH; C_b, 500 μF
SC: Capacity; terminal voltage; no. of batteries in series; peak current; continuous current; Converter parameters	C_{sc}, 58 F, V_{sc}, 12; 4; I_p, 200 A; I_{msc}, 19 A; L_{sc}, 5 mH; C_{sc}, 500 μF
DC grid voltage	V_{dc}, 80 V

is no effect on the steady DC link voltage. The SoC of B1 and B2 responds to battery charging and discharging conditions in Figs. 18 and 19. show the DC grid voltage for RR and SR control is shown in Fig. 20(a) and (b) to evaluate the voltage drop and efficiency analysis at the DC link. Figs. 21 and 22 show the PV power output without smoothing controllers. The controller is implemented to limit the fluctuating PV power output changes to the desirable limit-rate value. Fig. 23 shows the ramp-rate and step-rate controls for smoothening PV power output. Figs. 24–26 shows the HIL results for PV power before and after using the smoothing controllers. The PV-RRC power output delivered to the grid is more than the PV-SRC power output. Hence, the PV-RRC method meets the amount of power required by the load. Thus, the size of ESS can be reduced when compared to the SRC method.

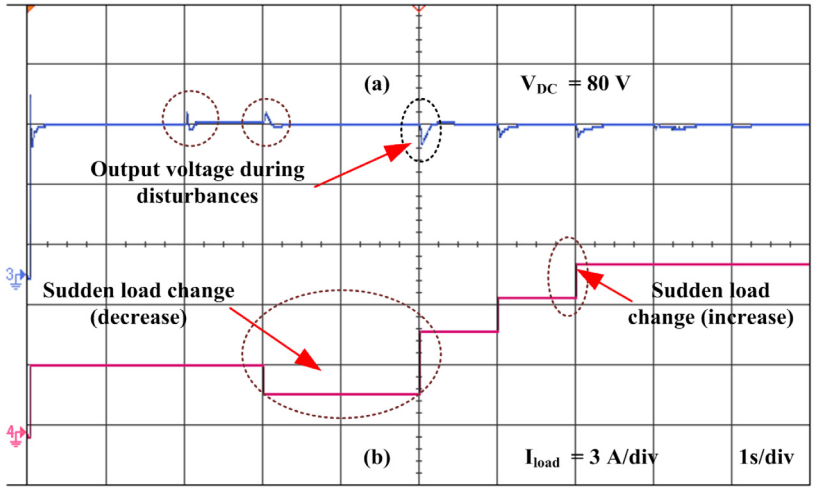

Fig. 14. HIL test-bench results — Ramp-Rate control: (a) DC-bus voltage (V_{DC}), (b) Load current (I_{load}).

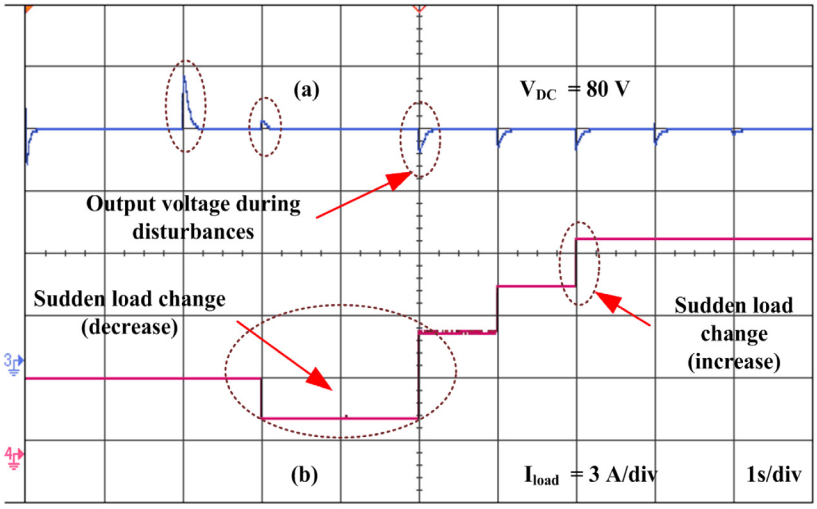

Fig. 15. HIL test-bench results — Step-Rate control: (a) DC-bus voltage (V_{DC}), (b) Load current (I_{load}).

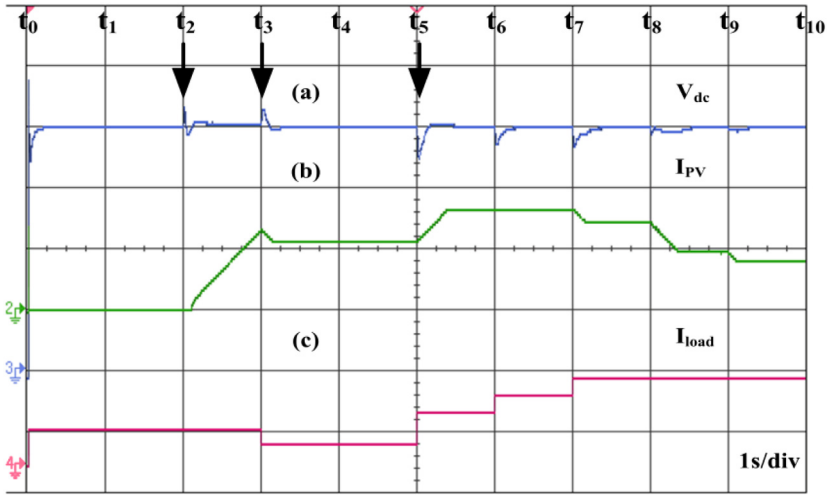

Fig. 16. HIL test-bench results — Ramp-rate control: (a) DC link voltage (V_{dc}), (b) PV current (I_{PV}), (b) load current (I_{load}).

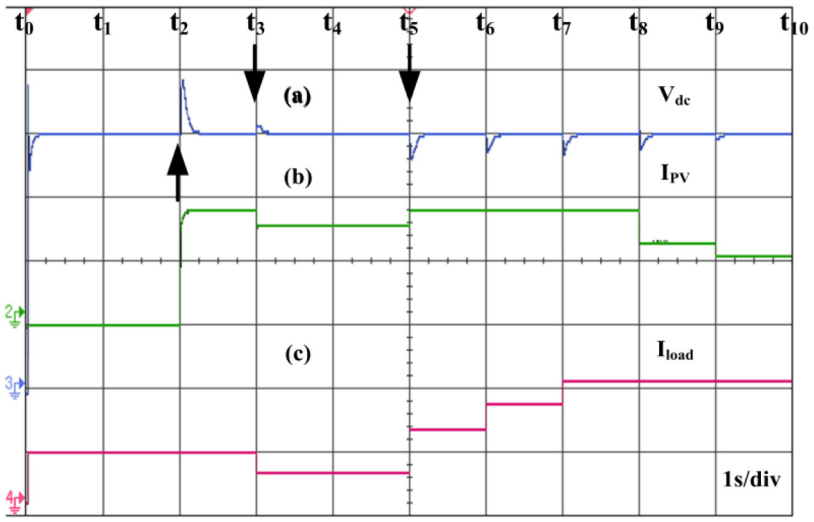

Fig. 17. HIL test-bench results — Step-rate control: (a) DC link voltage (V_{dc}), (b) PV current (I_{PV}), (b) load current (I_{load}).

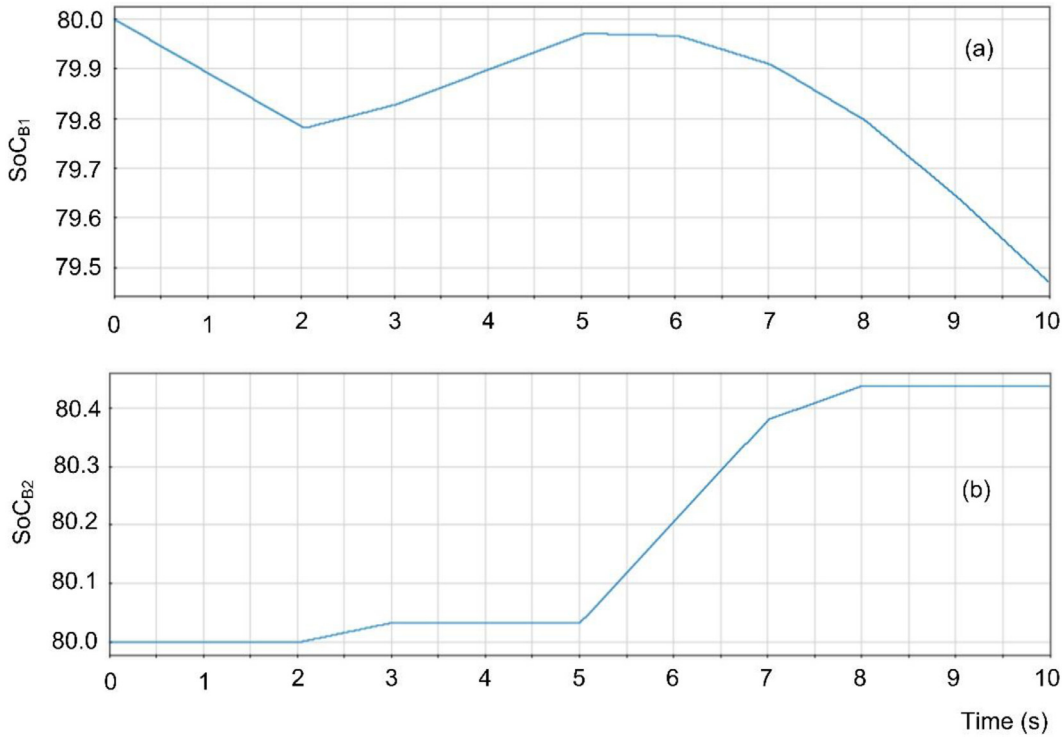

Fig. 18. Ramp-rate control: (a) battery-1 SoC (SoC_{B1}), (b) battery-2 SoC (SoC_{B2}).

Table 3
Performance of proposed system with existing methods.

Parameters index	Kollimalla et al. (2017)	Kotra and Mishra (2019)	Sathishkumar et al. (2012)	Proposed method (SR control)	Proposed method (RR control)
M_p (%)	6.25	3.7	5	6.25	2.25
T_s	300 ms	400 ms	900 ms	199 ms	199 ms

The above findings show that the RR control strategy provides faster voltage regulation than the existing methods presented in Table 3. As shown in Fig. 27, the settling time (T_s) is measured between t_1 and t_2, and the change in the voltage (ΔV_{dc}) is very low. Therefore, the proposed system can improve performance using RR control compared to existing methods. Also, the RR control method's current charge/discharge rate is low; it reduces current stress and improves battery life. In addition, battery size is significantly reduced as SC manages transient currents, and costs are reduced. The efficiency of the RR control strategy is higher than the SR control strategy, and it can be measured by the ratio of useful output to total input. In Table 4, the RR and

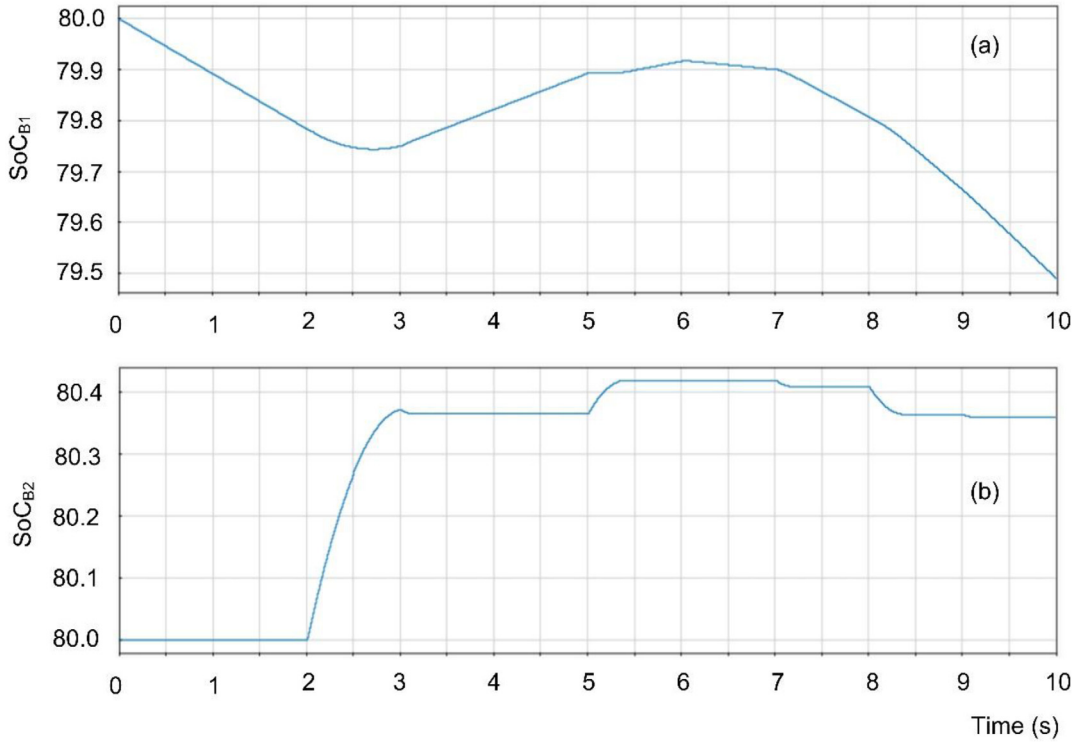

Fig. 19. Step-rate control: (a) battery-1 SoC (SoC_{B1}), (b) battery-2 SoC (SoC_{B2}).

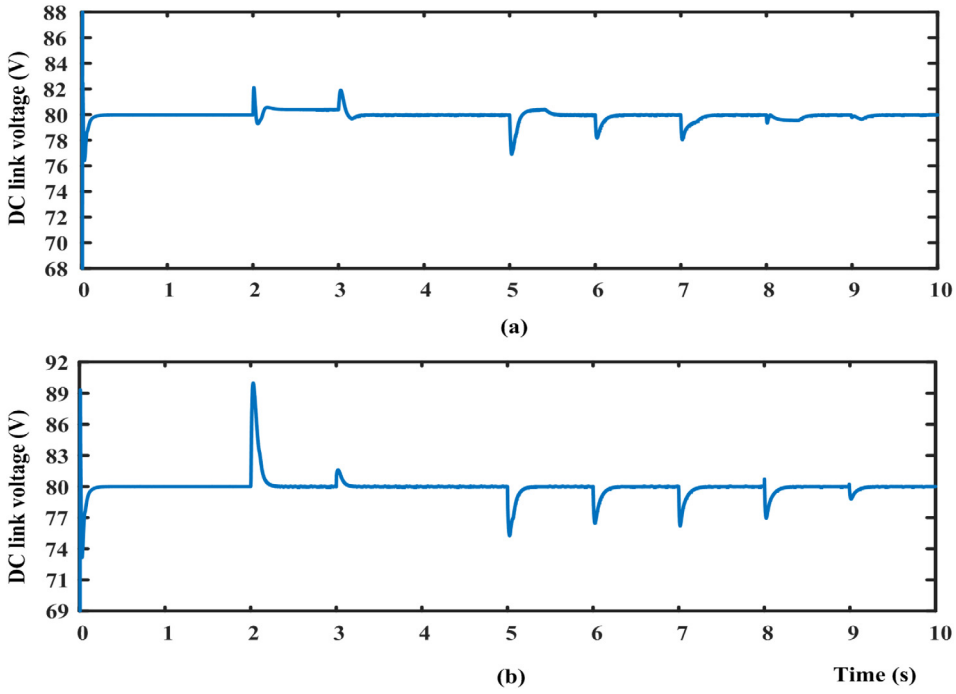

Fig. 20. Simulation results: (a) RR control DC link voltage, (b) SR control DC link voltage.

SR controls are compared. The RR control strategy is observed to be more effective in terms of efficiency, voltage drop, losses, SoC levels, cycling degradation, and voltage regulation at the DC link.

6. Conclusion

This paper analyzed the storage requirements for smoothing fluctuations in PV power based on the RR and SR control strategies. A simulation analysis was performed under the same irradiance profile conditions. This profile is distinguished by high solar variability, which aids in mapping results obtained under the same irradiance variability conditions. The RR controller requires less battery energy than the SR and has fewer cycles than other smoothing methods. RR control achieves faster DC link voltage regulation and lower voltage drop than the SR control method. The system's efficiency using the RR method is 98.07

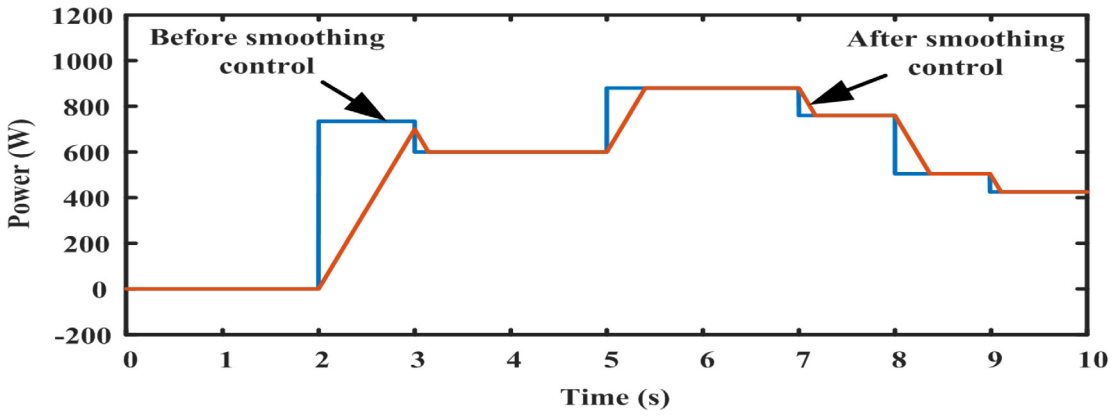

Fig. 21. Simulation results: PV power output before and after using ramp-rate control.

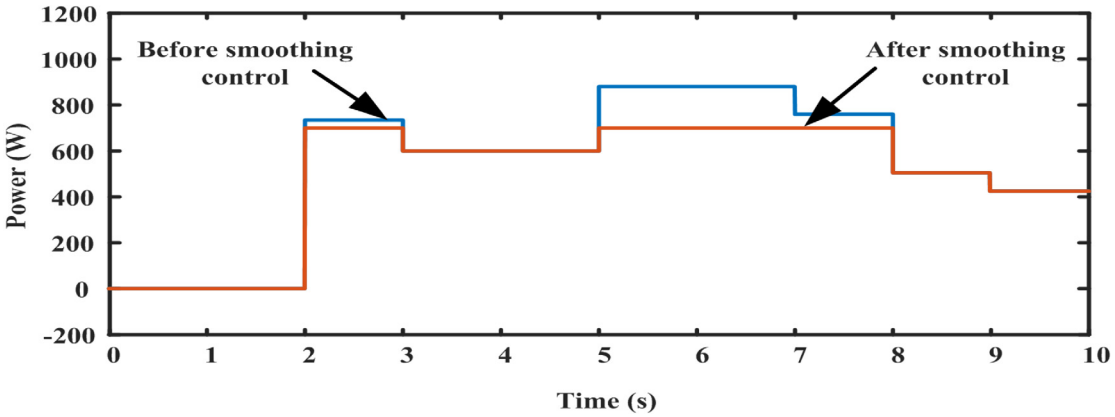

Fig. 22. Simulation results: PV power output before and after using step-rate control.

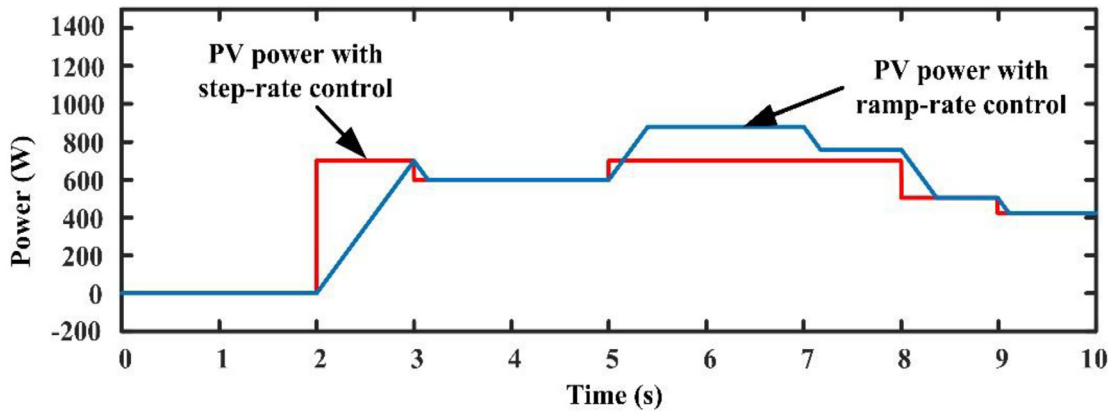

Fig. 23. Simulation results: Comparison of PV power output with ramp-rate and step-rate smoothing controls.

Table 4
Analysis of voltage drop and efficiency for RR and SR control methods.

Time interval (s)	$V_{dc,change}$ (±) (Ramp-rate)	Efficiency (%)	$V_{dc,change}$ (±) (Step-rate)	Efficiency (%)
t_2	2 V	97.5	10 V	87.5
t_3	1 V	98.75	2 V	97.5
t_5	3 V	96.25	6 V	92.5
t_6	1.8 V	97.75	5 V	93.75
t_7	2 V	97.5	5 V	93.75
t_8	0.5 V	99.375	5 V	93.75
t_9	0.5 V	99.375	2 V	97.5

percent, while the system's efficiency using the SR method is about 95.6 percent. Compared to the SR method, the RR controller is more effective in regulating the output of the batteries to minimize variations in output PV power and maintain power balance at the DC link. The effectiveness of storage time is much higher in the RR method than in the SR control method because it responds quickly to changes in demand and charges. The overall performance analysis of the control methods presented in the paper is evaluated in Table 5. Although various methods have been evaluated for smoothing over a single radiation day, a better understanding of the overall lifetime operation of the battery is required. Future research aims to develop a lifespan model to understand these issues better.

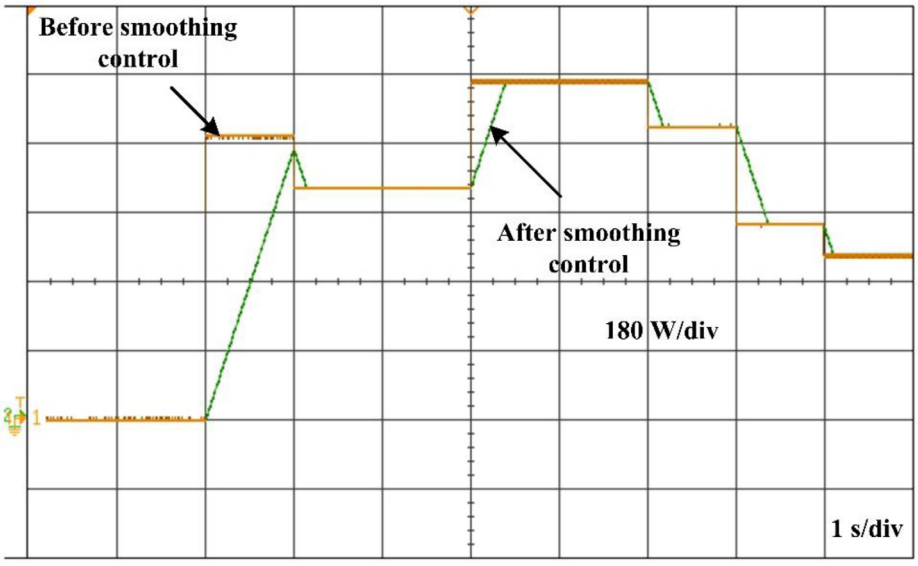

Fig. 24. HIL results: PV power output before and after using ramp-rate control.

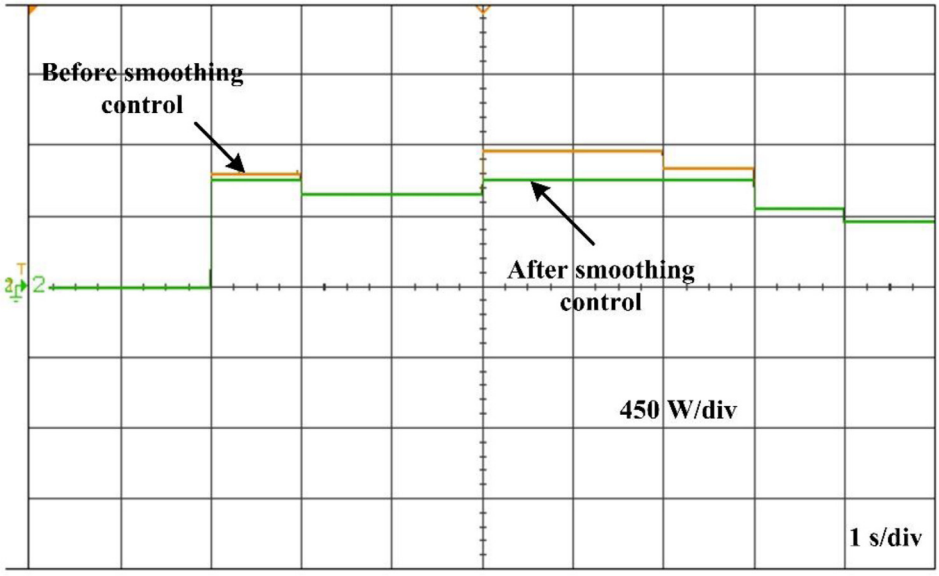

Fig. 25. HIL results: PV power output before and after using step-rate control.

Table 5
Performance analysis of RR and SR control methods in DC MG system.

Control strategy	Storage efficiency	System losses	% Drop in DC grid voltage	System efficiency	Storage time effectiveness	Voltage regulation at the DC link	Charging/discharging of storage
RR strategy	High	Low	Exceptionally low	High	Particularly good	Fast	Most efficient
SR strategy	Average	Average	Low	Medium	Good	Medium	Medium efficient

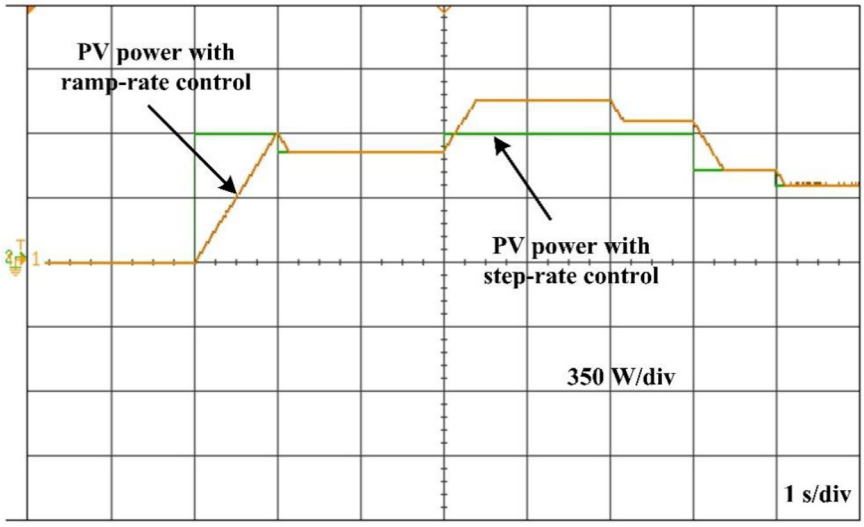

Fig. 26. HIL results: Comparison of PV power output with ramp-rate and step-rate smoothing controls.

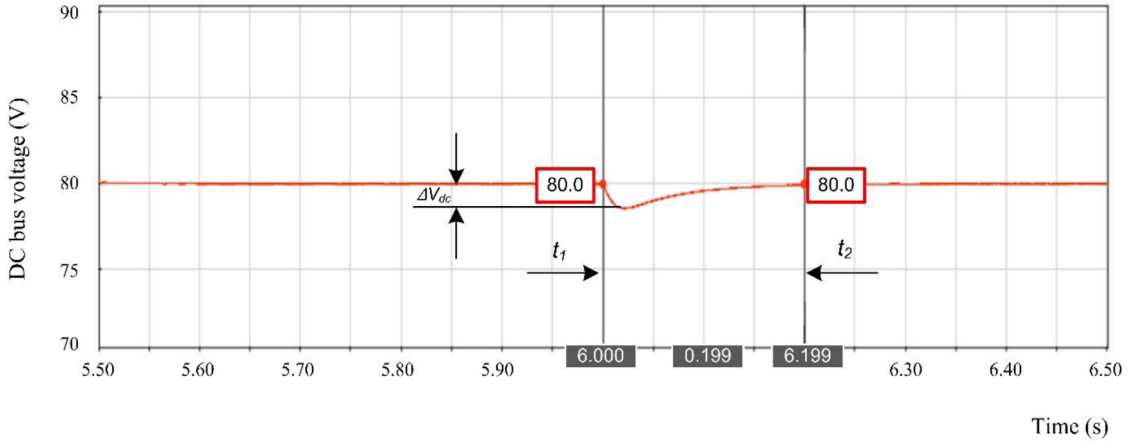

Fig. 27. Performance of the DC bus voltage in the proposed system.

CRediT authorship contribution statement

G.V. Brahmendra Kumar: Investigation, Execution of the work, Performed the numerical simulation and hardware testing to validate the proposed configuration, Edited the manuscript and prepared the high-resolution figures and experimental results for its quality presentation, Reviewed the manuscript and were involved in making an error-free version of the grammar. **Palanisamy K.:** Investigation, Execution of the work, Performed the numerical simulation and hardware testing to validate the proposed configuration, Edited the manuscript and prepared the high-resolution figures and experimental results for its quality presentation, reviewed the manuscript and were involved in making an error-free version of the grammar. **Sanjeevikumar P.:** Investigation, Execution of the work, Performed the numerical simulation and hardware testing to validate the proposed configuration, Edited the manuscript and prepared the high-resolution figures and experimental results for its quality presentation, reviewed the manuscript and were involved in making an error-free version of the grammar, Work fully supervised for its quality work in presentation and addressed new information for readers. **S.M. Muyeen:** Investigation, Execution of the work, Performed the numerical simulation and hardware testing to validate the proposed configuration, Edited the manuscript and prepared the high-resolution figures and experimental results for its quality presentation, reviewed the manuscript and were involved in making an error-free version of the grammar, Work fully supervised for its quality work in presentation and addressed new information for readers.

Declaration of competing interest

The authors declare that they have no known competing financial interests or personal relationships that could have appeared to influence the work reported in this paper.

Data availability

No data was used for the research described in the article.

Acknowledgments

This work is supported by the Department of Science and Technology (DST), Government of India (GOI), with the project grant SR/FST/ETI-420/2016(C) under the FIST scheme. Open Access funding provided by the Qatar National Library.

References

Beltran, H., Tomás García, I., Alfonso-Gil, J.C., Pérez, E., 2019. Levelized cost of storage for Li-Ion batteries used in PV power plants for ramp-rate control. IEEE Trans. Energy Convers. 34, 554–561.

Brahmendra Kumar, G.V., Kumar, G.A., Eswararao, S., Gehlot, D., 2018. Modeling and control of bess for solar integration for PV ramp rate control. In: Proceedings of the 2018 International Conference on Computation of Power, Energy, Information and Communication. ICCPEIC, India, pp. 368–374.

Brahmendra Kumar, G.V., Palanisamy, K., 2019. A review on microgrids with distributed energy resources. In: 2019 Innovations in Power and Advanced Computing Technologies (I-PACT). India, pp. 1–6. http://dx.doi.org/10.1109/i-PACT44901.2019.8960189.

Brahmendra Kumar, G., Palanisamy, K., 2021. Review of energy storage system for microgrid. In: Microgrid Technologies. Wiley publications, pp. 57–90. http://dx.doi.org/10.1002/9781119710905.ch3.

Cao, J., Du, W., Wang, H.F., Mcculloch, MD., 2018. Optimal sizing and control strategies for hybrid storage system as limited by grid frequency deviations. IEEE Trans. Power Syst. 33, 5486–5495.

Chen, X., Du, Y., Wen, H., Jiang, L., Xiao, W., 2019. Forecasting-based power ramp-rate control strategies for utility-scale PV systems. IEEE Trans. Ind. Electron. 66, 1862–1871.

Gundumalla, V.B.K., Eswararao, S., 2018. Ramp rate control strategy for an islanded DC microgrid with hybrid energy storage system. In: 2018 4th International Conference on Electrical Energy Systems. ICEES, pp. 82–87.

Kollimalla, S.K., Mishra, M.K., Ukil, A., Gooi, HB., 2017. DC grid voltage regulation using new HESS control strategy. IEEE Trans. Sustain. Energy 8 (2), 772–781.

Kotra, S., Mishra, M.K., 2019. Design and stability analysis of DC microgrid with hybrid energy storage system. IEEE Trans. Sustain. Energy 10 (3), 1603–1612.

Kumar, G.V.B., Kaliannan, P., Padmanaban, S., Holm-Nielsen, J.B., Blaabjerg, F., 2020. Effective management system for solar PV using real-time data with hybrid energy storage system. Appl. Sci. 10, 1–15.

Kumar, G.V.B., Palanisamy, K., 2019. Interleaved boost converter for renewable energy application with energy storage system. In: Proceedings of the 2019 IEEE 1st International Conference on Energy, Systems, and Information Processing. ICESIP, India, pp. 1–5.

Kumar, G.V.B., Palanisamy, K., 2020. A review of energy storage participation for ancillary services in a microgrid environment. Inventions 5, 1–36.

Kumar, G.V.B., Palanisamy, K., 2021. Deployment of energy storage system for current microgrid environment: An overview. In: 2021 Innovations in Power and Advanced Computing Technologies (I-PACT). pp. 1–6. http://dx.doi.org/10.1109/i-PACT52855.2021.9697061.

Lamsal, D., Sreeram, V., Mishra, Y., Kumar, D., 2019. Smoothing control strategy of wind and photovoltaic output power fluctuation by considering the state of health of battery energy storage system. IET Renew. Power Gener. 13 (4), 578–586.

Li, X., Wen, H., Chen, B., Ding, S., Xiao, W., 2020. A cost-effective power ramp rate control strategy based on flexible power point tracking for photovoltaic systems. Sol. Energy 208, 1058–1067.

Lin, D., Li, X., Ding, S., Du, Y., 2020. Strategy comparison of power ramp rate control for photovoltaic systems. CPSS Trans. Power Electron. Appl. 5 (4), 329–341.

Mahmud, N., Zahedi, A., Mahmud, A., 2017. A cooperative operation of novel PV inverter control scheme and storage energy management system based on ANFIS for voltage regulation of grid-tied PV system. IEEE Trans. Ind. Inform. 13 (5), 2657–2668.

Mardani, M.M., Khooban, M.H., Masoudian, A., Dragičević, T., 2019. Model predictive control of DC–DC converters to mitigate the effects of pulsed power loads in naval DC microgrids. IEEE Trans. Ind. Electron. 66, 5676–5685.

Neto, P.J., Barros, T.A., Silveira, J.P., Filho, E.R., Vasquez, J.C., Guerrero, J.M., 2020. Power management strategy based on virtual inertia for DC microgrids. IEEE Trans. Power Electron. 35, 12472–12485.

Patel, S., Ahmed, M., Kamalasadan, S., 2020. A novel energy storage-based net-load smoothing and shifting architecture for high amount of photovoltaics integrated power distribution system. IEEE Trans. Ind. Appl. 56, 3090–3099.

Prabha, MA., Kashem, M.M., Danny, S., 2019. The simultaneous mitigation of slow and fast voltage fluctuations caused by rooftop solar PV by controlling the charging/discharging of an integrated battery energy storage system. J. Energy Storage 26, 1–11.

Pranith, S., Kumar, S., Singh, B., Bhatti, T.S., 2022. MAF-DCGI based single-phase uninterrupted PV-battery system under unintentional islanding. IEEE Trans. Energy Convers. 37 (1), 36–49.

Saleh, M., Meek, L., Masoum, MA., Abshar, M., 2018. Battery-less short-term smoothing of photovoltaic generation using sky camera. IEEE Trans. Ind. Inform. 14, 403–414.

Sathishkumar, R., Kollimalla, S.K., Mishra, M.K., 2012. Dynamic energy management of microgrids using battery super capacitor combined storage. In: 2012 Annual IEEE India Conference. INDICON, pp. 1078–1083.

Schnabel, J., Valkealahti, S., 2016. Energy storage requirements for PV power ramp rate control in Northern Europe. Int. J. Photoenergy 2016, 1–11.

Solomon, A.A., Bogdanov, D., Breyer, C., 2019. Curtailment-storage-penetration nexus in the energy transition. Appl. Energy 235, 1351–1368.

Sukumar, S., Marsadek, M., Agileswari, K.R., Mokhlis, H., 2018. Ramp-rate control smoothing methods to control output power fluctuations from solar photovoltaic (PV) sources—A review. J. Energy Storage 20, 218–229.

Tahir, H., Park, D., Park, S., Kim, R., 2022. Optimal ESS size calculation for ramp rate control of grid-connected microgrid based on the selection of accurate representative days. Int. J. Electr. Power Energy Syst. 139, 1–13.

Tummuru, N.R., Mishra, M.K., Srinivas, S., 2015. Dynamic energy management of renewable grid integrated hybrid energy storage system. IEEE Trans. Ind. Electron. 62 (12), 7728–7737.

Xu, Q., Xiao, J., Wang, P., Pan, X., Wen, C., 2017. A decentralized control strategy for autonomous transient power sharing and state-ofcharge recovery in hybrid energy storage systems. IEEE Trans. Sustain. Energy 8 (4), 1443–1452.

Zeraati, M., Hamedani Golshan, M.E., Guerrero, J.M., 2018. Distributed control of battery energy storage systems for voltage regulation in distribution networks with high PV penetration. IEEE Trans. Smart Grid 9 (4), 3582–3593.

Zhang, D., Chen, Y., Wang, L., Liu, J., Yuan, R., Wu, J., Zhang, Y., Li, M., 2021. Control strategy and optimal configuration of energy storage system for smoothing short-term fluctuation of PV power. Sustain. Energy Technol. Assess. 45, 1–9.